PCCP

Accepted Manuscript

This is an *Accepted Manuscript*, which has been through the Royal Society of Chemistry peer review process and has been accepted for publication.

Accepted Manuscripts are published online shortly after acceptance, before technical editing, formatting and proof reading. Using this free service, authors can make their results available to the community, in citable form, before we publish the edited article. We will replace this *Accepted Manuscript* with the edited and formatted *Advance Article* as soon as it is available.

You can find more information about *Accepted Manuscripts* in the **Information for Authors**.

Please note that technical editing may introduce minor changes to the text and/or graphics, which may alter content. The journal's standard **Terms & Conditions** and the **Ethical guidelines** still apply. In no event shall the Royal Society of Chemistry be held responsible for any errors or omissions in this *Accepted Manuscript* or any consequences arising from the use of any information it contains.

ARTICLE

Formation and decay of charge carriers in aggregate nanofibers consisting of poly(3-hexylthiophene)-coated gold nanoparticles

Dongki Lee,[a] Jaewon Lee,[a] Ki-Hee Song,[b] Hanju Rhee,[b] and Du-Jeon Jang[a,*]

Thin nanofibers (NFs) of J-dominant aggregates having thickness of 15 nm and thick NFs of H-dominant aggregates having thickness of 25 nm have been fabricated by self-assembling poly(3-hexylthiophene)-coated gold nanoparticles. The formation and decay dynamics of charge carriers, which are dependent on the aggregate types of NFs, has been investigated by time-resolved emission and transient-absorption spectroscopy. With increasing excitation energy, the fraction of the fast emission decay component has been found to decrease, suggesting that the fast formation of polaron pairs (PP), localized (LP), and delocalized polarons (DP) results from higher singlet exciton states produced by the singlet fusion. The faster decay dynamics of DP and LP in thick NFs than in thin NFs is due to the increased delocalization of DP and LP. As interchain aggregation is weaker than intrachain aggregation, PP decays faster in thin NFs than in thick NFs. In both thin and thick NFs, whereas triplet (T_1) excitons have been hardly observed with excitation at 532 nm on a nanosecond time scale, they have been observed with excitation at 355 nm, revealing that T_1 excitons within NFs are mainly generated through the singlet fission from a higher singlet exciton state rather than through intersystem crossing.

1. Introduction

The design and controlled fabrication of nanostructured materials having functional properties have been extensively studied.[1-4] In particular, hybrid nanocomposites consisting of conjugated polymers and inorganic materials have received intense attention for applications in optoelectronic devices such as light-emitting diodes, biosensors, and photovoltaic cells because of their ability to provide diverse opportunities for the development of novel nanomaterials having improved physical and chemical properties against single-component counterparts.[5-8] Among numerous conjugated polymers, poly(3-hexylthiophene) (P3HT), which is most commonly used in optoelectronic devices, has been extensively studied because of its facilely tunable optical and electrical properties controlled by regulating the conformation, packing, and morphology of individual chains.[9-12] The modification of the hexyl substitution changes the solubility of the polymer to make P3HT self-assembled into a two-dimensional high-interchain lamella with favorable head-to-head (HH) coupling or into a one-dimensional (1D) high-intrachain nanostructure with unfavorable HH coupling, depending on diverse formation

conditions such as the degree of regioregularity[13-15] and the types of solvents.[16-19] Especially, since 1D nanostructures, namely nanofibers (NFs), of P3HT have good advantages such as large surface areas and 1D path ways at the nanosized level for the migration of charge carriers, they are expected to have improved optoelectronic device performances.[20-24] The dynamics of charge carriers generated from the excited states of P3HT within NFs plays an important role on device performances and is heavily influenced by conformational behaviors of P3HT chains. Therefore, not only a fundamental understanding of the photophysics of non-aggregate individual P3HT chains but also the comprehensive investigation of photoinduced charge carriers affected by the types of aggregate NFs are critical research points in diverse optoelectronic application fields where P3HT is used.[25-32]

Aggregates of conjugated polymers can be distinguished by two types of fundamental electronic interactions: one occurring within a given chain and the other occurring between chains.[33a] The impact of such excitonic interactions on the photophysics of polymer films can be understood using the concepts of J- and H-aggregation. In polymer assemblies, intrachain head-to-tail (HT) through-bond interactions lead to J-aggregate behaviors, whereas interchain Coulombic HH interactions lead to H-aggregate behaviors.[33] Different coupling types of J- and H-aggregates are readily distinguished by intensity difference between the origin (0–0) transition and the sideband (0–1, or higher) vibronic transitions. When interchain HH order is dominant in H-aggregate NFs, the 0-0 electronic transition is forbidden by symmetry and less intense than the 0-1 vibronic sideband. In contrast, when intrachain HT order is dominant in J-aggregate NFs, the 0-0 transition is

[a] *Department of Chemistry, Seoul National University, Seoul 08826, Korea*
[b] *Space-Time Resolved Molecular Imaging Team, Korea Basic Science Institute, Seoul 02841, Korea*
*Corresponding author. TEL: +82 2 880 4368; FAX: +82 2 875 6624. E-mail address: djjang@snu.ac.kr.

allowed and more intense than the 0-1 vibronic sideband.[33-36] In H-aggregate systems, typical in most thin films, the 0–0 transition in emission is weakly allowed due to structural or thermal disorder, and most of the emission intensity is carried in the 0–1 vibronic transition. This gives rise to 0–0/0–1 intensity ratios smaller than 1 for H-aggregate systems. Conversely, the rigid linear arrangement of thiophene units results in dominant intrachain coupling manifested as J-aggregate behaviors, where the 0–0 transition is strongly allowed, thus giving rise to 0–0/0–1 intensity ratios larger than 1.[37,38]

Diverse recent spectroscopic studies on aggregate P3HT systems have shown that the formation and decay of charge carriers such as excitons and polarons are strongly dependent on the aggregate behaviors of P3HT chains.[11-15,34-37,39,40] Grey et al.[11] have demonstrated that a triplet exciton can also form via a recombination of long-lived polarons in J-aggregate NFs having high intrachain order. High intrachain order in J-aggregate P3HT NFs facilitates the delocalization of siglet excitons, leading to the eventual formation of triplet excitons via the nongeminate recombination of delocalized polaron species. The formation and decay dynamics of triplet excitons and polarons has been reported[13,14] to depend on the regioregularity of P3HT films. Because of strong interchain interactions in regioregular P3HT films, singlet excitons are more delocalized to form interchain excitons, whereas intrachain singlet excitons formed in regiorandom P3HT films are substantially converted to triplet excitons through the singlet fission.[13] Although previous studies[13,14] have provided useful information on charge carriers generated in aggregate P3HT systems, the formation and decay dynamics of charge carriers dependent on aggregate types in aggregate P3HT NFs has not been fully understood over the wide wavelength region from the visible to the near infrared.
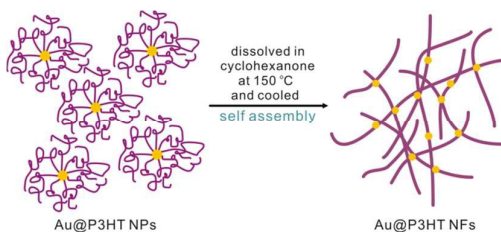
Scheme 1. Schematic for the fabrication of Au@P3HT NFs.

In this paper, we present that NFs with H-dominant and J-dominant aggregates have been fabricated by self-assembling P3HT-coated gold nanoparticles (Au@P3HT NPs) in cyclohexanone (Scheme 1 and Fig. S1 of ESI†). The picosecond dynamics of charge carriers such as singlet (S_1) and triplet excitons (T_1), polaon pairs (PP), and localized (LP) and delocalized polarons (DP) of H-aggregate-dominant NFs with thickness of 25 nm (thick NFs) and J-aggregate-dominant NFs with thickness of 15 nm (thin NFs) has been also investigated using time-resolved emission and transient-absorption (TA) spectroscopy (Scheme 2). To understand the role of gold nanoparticles (Au NPs) within NFs, we have also fabricated

pristine NFs using Au NPs-free pristine P3HT via the same preparation procedure of thin NFs. The decay time constants of S_1 excitons in thick NFs are found to be smaller than those in thin NFs due to the increase of interchain stacking effects. With increasing excitation energy, the fraction of the fast emission decay component has been found to decrease, suggesting that the fast formation of PP, LP, and DP results from higher singlet exciton states. The faster decay dynamics of LP and DP in thick NFs indicates that the interchain delocalization effect is predominant. However, as interchain aggregation is weaker than intrachain aggregation, PP decays faster in thin NFs than in thick NFs. In both thin and thick NFs, T_1 excitons were hardly observed with excitation at 532 nm. On the other hand, they have been observed with excitation at 355 nm, revealing that T_1 excitons in NFs mainly arise from the singlet fission of a higher singlet exciton state.
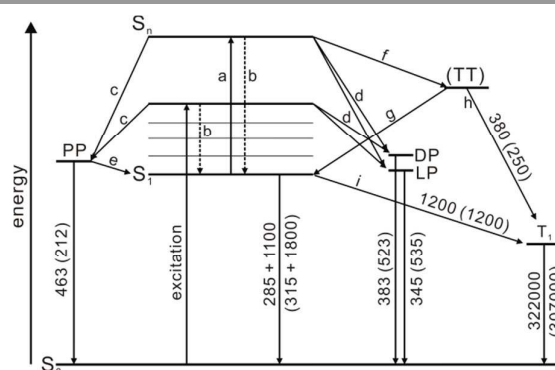
Scheme 2. Schematic representation for the dynamics of singlet (S_1) and triplet excitons (T_1), triplet pairs (TT), localized (LP) and delocalized polarons (DP), polaron pairs (PP) in thick (thin) Au@P3HT NFs, where time constants are indicated in the units of ps. Key: [a] singlet fusion, [b] vibrational relaxation, [c] PP formation, [d] LP or DP formation, [e] geminate recombination to S_1, [f] singlet fission, [g] triplet fusion, [h] T_1 formation, and [i] intersystem crossing.

2. Experimental section

2.1 Synthesis

The detailed synthetic and characterization procedures of P3HT-functionalized gold nanoparticles (Au@P3HT NPs) have already been reported.[30] Thin and thick NFs were prepared in a poor solvent via a self-assembly process, as described in detail elsewhere.[20,22] For the fabrication of thin NFs, 4.0 mg of Au@P3HT NPs was dissolved in 10 mL of cyclohexanone (l, 99%, Sigma-Aldrich) in a 50 mL three-neck reaction vessel. The colloid was slowly heated to 150 °C and kept in the dark under N_2 atmosphere. The mixture was turned into a homogeneous limpid orange-colored solution and then cooled to room temperature naturally to generate self-assembled NFs. Then, the produced opaque violet-colored colloidal solution was centrifuged for 30 min at 13,500 rpm. The supernatant was discarded and the precipitated NFs were dispersed in 0.5 mL of cyclohexanone. The preparation procedure of thick NFs was the same as that of thin NFs, except that the weight of Au@P3HT NPs was increased three times.

2.2 Characterization

Transmission electron microscopy (TEM) images were obtained with a Hitachi H7600 microscope; a TEM sample was prepared by evaporating and drying a colloidal droplet on a carbon-coated copper grid in an argon glovebox at room temperature. Scanning electron microscopy (SEM) images were obtained with a JEOL-6700F microscope; the same TEM samples were also used for SEM measurements. Atomic force microscopy (AFM) images were obtained with a Veeco Instrument MultiMode 8 and Nanoscope Ⅴ controller; AFM samples were prepared by spin-coating a colloidal drop for 30 s at 3,000 rpm on highly ordered pyrolytic graphite (HOPG) substrates, and the all images were obtained on tapping modes. While absorption spectra were measured with a Scinco S3100 UV/vis spectrophotometer, emission spectra were obtained using a home-built fluorometer consisting of a 75 W Acton Research XS 432 Xe lamp with an Acton Research Spectrapro150 monochromator of 0.15 m and an Acton Research PD438 photomultiplier tube attached to an Acton Research Spectrapro300 monochromator of 0.30 m.

2.3 Transient-Absorption (TA) and Emission Kinetics

For femtosecond TA measurements, a 40 fs pump beam and a 200 fs probe beam were generated from a non-collinear Light Conversion ORPHEUS-N optical parametric amplifiers (OPA) and a collinear Light Conversion ORPHEUS OPA, respectively, and amplified using a Light Conversion PHAROS Yb:KGW-doped regenerative amplifier with a repetition rate of 1 kHz. The pump was tuned to a fixed wavelength of 355 nm and the probe over a wide wavelength region from the visible to the near infrared. Time delays between the pump and the probe pulses were controlled with a Newport M-ILS150CC motorized linear delay stage. Whereas both the pump (10 nJ) and the probe (1 nJ) pulses were focused into a sample by a CaF2 lens with a focal length of 10 cm, only the probe beam was then detected by a Si 350-1100 nm photodiode with the pump blocked. The pump and the probe polarizations were set to be the same. To remove light scattered from the pump beam and the residual second harmonic of the probe beam, long-pass filters with variable-wavelength cut-off filters were used in front of the detector. For the phase-sensitive detection of the pump-induced TA signal, the pump beam was modulated by an optical chopper synchronized at a sub-harmonic frequency (500 Hz) of the laser repetition rate and the modulated probe signal was finally recorded at a Stanford Research Systems SR830 lock-in amplifier via a Stanford Research Systems SR250 gated integrator. Nanosecond TA and picosecond emission kinetic profiles were obtained as described in a previous report.[30]

3 Results and discussion
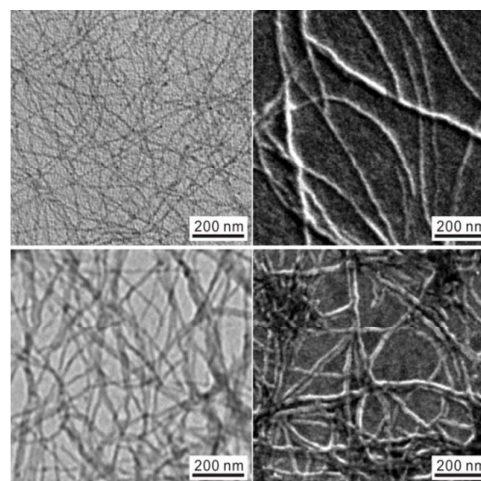
Fig. 1 TEM (left) and SEM images (right) of thin (top) and thick NFs (bottom).

TEM and SEM images of thin and thick NFs prepared by evaporating a droplet of dilute thin or thick NFs dispersed in cyclohexanone on a carbon-coated copper grid are shown in Fig. 1. AFM images of thin and thick NFs are also shown in Fig. S2 of ESI†. The morphology of thin NFs has the network structure of silk fibers with thickness of 15±2 nm, whereas that of thick NFs has the network structure of blood vessels with thickness of 25±6 nm. As shown in Fig. S1 of SI†, the formation mechanisms of NFs have been proposed to depend on two critical factors: the concentration of Au@P3HT NPs in cyclohexanone and the chemical-bond interactions of thiol-terminated P3HT (P3HT-SH) with gold NPs.[30] With the concentration increase of Au@P3HT NPs in cyclohexanone, the thickness of NFs increases and the morphology of NFs becomes more complicated, suggesting that the dominant tendency of aggregation during the formation of NFs changes from a intrachain aggregate along the transverse axis into a interchain aggregate along the longitudinal axis. As a result, thin NFs having thickness of 15±2 nm have been predominantly formed along the transverse axis at a low concentration to have folded or extended polymer backbones extensively. On the other hand, thick NFs having thickness of 25±6 nm have been prevailingly formed along the longitudinal axis at a high concentration to have stacked polymer backbones abundantly. The formation kinetics of NFs as well as the molecular weight (M_n) of P3HT has been reported to play an important role in determining the dominant coupling types of aggregate P3HT NFs during the formation of NFs.[11,34] The rapid formation kinetics of NFs in a poor solvent such as anisole promotes H-type NFs, whereas the slow self-assembly process of P3HT chains over several days in toluene cultivates J-type NFs.[11] In the low M_n condition, H-type NFs are predominantly formed, and in the high M_n condition, J-type NFs are prevalently produced.[34] In our formation conditions of NFs, although we have chosen the rapid formation kinetics in a poor solvent such as cyclohexanone and P3HT-attached gold NPs having low M_n (10,565 g mol^{-1}),[30] J-aggregate-dominant NFs have been

abundantly formed in the low-concentration condition due to strong chemical-bond interactions between P3HT-SH and gold NPs, inducing the transverse aggregation rather than the longitudinal aggregation. Since the effect of chemical-bond interactions competes with the concentration effect of Au@P3HT NPs in the high-concentration condition, the longitudinal aggregation becomes as important as the transvers aggregation in the formation of thick NFs. Consequently, the thickness of NFs associated with transition in dominant exciton coupling from intrachain coupling to interchain coupling in NFs has been facilely tuned via controlling the concentration of Au@P3HT NPs in cyclohexanone, producing stable and well-ordered NFs with H-dominant and J-dominant aggregates homogeneously at the molecular level.
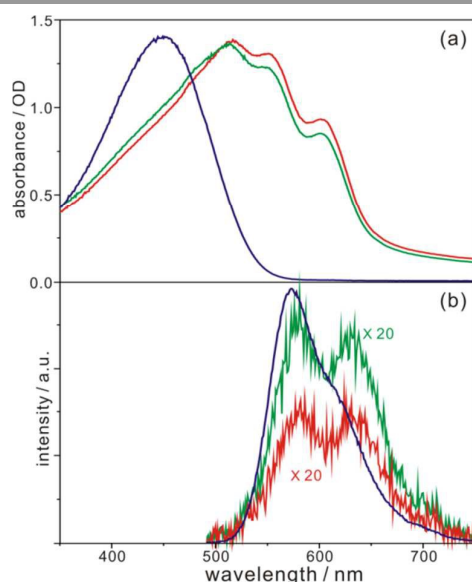
Fig. 2 Absorption (a) and emission spectra (b) of non-aggregate Au@P3HT NPs in chloroform (blue), thin NFs in cyclohexanone (green), and thick NFs in cyclohexanone (red). Samples were excited at 355 nm for the emission spectra.

Fig. 2a shows that the absorption spectra of thin and thick NFs in cyclohexanone are considerably different from the absorption spectrum of non-aggregated Au@P3HT NPs in chloroform. The absorption maxima of thin and thick NFs in cyclohexanone have been observed to shift to the red by 60 and 64 nm, respectively, from that of Au@P3HT NPs in chloroform due to the increased conjugation length of intrachain or interchain π-π transition in aggregated P3HT backbones.[11,12,30,34-40] Based on previous studies,[16,34] each absorption spectrum of thin and thick NFs in Fig. S3 of ESI† has been deconvoluted into five bands having the maxima at 448 (violet), 486 (blue), 523 (green), 559 (yellow), and 604 nm (red), as given in Table S1 of ESI†. The deconvoluted absorption spectrum of thin or thick NFs consists of two parts: a high-energy region of the violet and blue bands arising from the transition of free or amorphous chains and a low-energy region of the green, yellow, and red bands originating from the

0-2 (A_{0-2}), 0-1 (A_{0-1}), and 0-0 vibronic transitions (A_{0-0}), respectively, of aggregated chains.[16]

Information on the dominant coupling type, H-type (interchain aggregate) or J-type (intrachain aggregate) is related to the intensity ratio of the origin (0-0) and the first-vibronic (0-1) transitions according to eq 1[16,33,35a]

$$\frac{A_{0-0}}{A_{0-1}} = \left(\frac{1 - 0.24 W/\omega_0}{1 + 0.073 W/\omega_0} \right)^2 \tag{1}$$

where W is the exciton bandwidth and ω_0 is the vibrational energy of the symmetric vinyl stretch. Since the exciton bandwidth is related to the strength of excitonic coupling between neighboring chains, the dominant coupling type of NFs can be readily figured out by intensity difference between the 0-0 and the 0-1 vibronic transitions of absorption spectra. The 0-0 transition and the 0-1 vibronic transition within aggregated NFs are restrained by selection rules. In H-type NFs, the 0-0 transition is forbidden because antiparallel transition dipole moments ($\Sigma\mu = 0$) are formed in the lower of two excited states. However, the 0-1 vibronic transition is allowed because parallel transition dipole moments ($\Sigma\mu \neq 0$) are formed in the higher of two excited states. On the other hand, the 0-0 transition is allowed in J-type NFs since head-to-tail aggregation causes parallel dipole moments ($\Sigma\mu \neq 0$) in the lower of two excited states. Because antiparallel transition dipole moments ($\Sigma\mu = 0$) are formed in the higher of two excited states, the 0-1 transition is forbidden in J-type NFs.[33-36,38]

The apparent absorbance ratio, A_{0-0}/A_{0-1}, of the 0-0 transition to the 0-1 vibronic transition in thin NFs (2.3) is 1.9 times greater than that in thick NFs (1.2) (Table S1 of ESI†). As discussed in the formation mechanisms of NFs (Fig. S1 of ESI†), the intrachain-aggregation effect is predominant in the low-concentration condition, resulting in J-aggregate-dominant NFs (thin NFs), whereas the interchain-aggregation effect is competitive in the high-concentration condition, resulting in H-aggregate-dominant NFs (thick NFs). Thus, the absorption spectra of NFs in Fig. 2a also support that the J-aggregate character is predominant in thin NFs due to the effect of intrachain aggregation along the transverse axis, whereas the H-aggregate character becomes as important as the J-aggregate character in thick NFs due to the increase of interchain interactions along the longitudinal axis between neighboring chains. To understand the role of Au NPs within NFs, we have also fabricated pristine NFs using Au NPs-free pristine P3HT via the same preparation procedure of thin NFs. The absorption spectra of Fig. S4 of ESI†, as well as Table S1 of ESI†, show increased absorption around 480 nm for pristine NFs, suggesting that the structure of pristine NFs is more amorphous than that of thin NFs because the chemical-bond interactions of P3HT-SH with gold NPs inducing highly transverse aggregation do not exist.

As shown in Fig. 2b, unlike the emission spectrum of non-aggregated Au@P3HT NPs in chloroform, each emission spectrum of thin and thick NFs in cyclohexanone has two characteristic bands at 650 and 690 nm and the emission

intensity of NFs is ~20 times weaker than that of NPs. The drastic quenching of emission is indicative of the existence of well-ordered aggregated P3HT chains and strong exciton coupling in NFs. The emission spectra of aggregate P3HT NFs with two featured peaks, the 0-0 transition at 650 nm and the 0-1 vibronic transition at 690 nm, have been numerously investigated[33-40] to distinguish the dominant coupling type.

Fig. 3 Emission spectra (black) of thin (a) and thick NFs (b) in cyclohexanone with excitation at 355 nm, fitted with three Gaussian curves λ_1 (blue), λ_2 (green), and λ_3 (red); violet curves represent the sum of the three fitted curves.

Fig. 3 shows that each emission spectrum of thin and thick NFs with excitation at 355 nm has been deconvoluted into three Gaussian curves having the maxima at 579 (blue), 635 (green), and 677 nm (red), as given in Table 1. The blue curves are ascribed to the recombination of relaxed S_1 excitons to the ground state of free or amorphous chains. On the other hand, the green curves are attributed to transition from the lowest-excited singlet state to the lowest vibrational level of the ground state (0-0 transition) of aggregated chains, and the red curves are due to transition from the lowest-excited singlet state to the first-excited vibrational level of the ground state (0-1 transition) of aggregated chains.[33,34,38] As mentioned with the absorption spectra of NFs, the dominant coupling type of NFs can be also easily figured out by intensity difference between the 0-0 transition and the 0-1 vibronic transition of emission spectra.[34,35] It has been reported[34] that the $I_{em}^{0-0}/I_{em}^{0-1}$ value of 65 kDa P3HT NFs having the strong J-type coupling is 1.8 while the value of 13 kDa P3HT NFs having the weak H-type coupling is 0.88. In our NFs, the apparent $I_{em}^{0-0}/I_{em}^{0-1}$ of thin NFs (4.2) is 2.5 times greater than that of thick NFs (1.7). Like the absorption spectra, this result also strongly supports that the J-aggregate character is predominant in thin NFs due to the effect of intrachain aggregation along the transverse axis, whereas the H-aggregate character becomes as important as the J-aggregate

character in thick NFs due to the increase of interchain interactions along the longitudinal axis between neighboring chains. Fig. S5 of ESI† shows that the 0-0 and the 0-1 transitions of aggregated chains around 630 and 690 nm, respectively, are much weaker than the respective ones of thin NFs due to the amorphous structure of pristine NFs, as discussed with the absorption spectra of Fig. S4 of ESI†.

Table 1. Three Gaussian Curves Fitted to Each Emission Spectrum of NFs Dispersed in Cyclohexanone

sample	λ_{ex} (nm)	λ_1^a (nm)	λ_2^b (nm)	λ_3^c (nm)
thin NFs	355	578±27 (48%)^d	635±25 (42%)	687±29 (10%)
thick NFs		580±28 (51%)	635±21 (31%)	668±36 (18%)
thin NFs	532	577±23 (37%)	632±28 (44%)	689±37 (19%)
thick NFs		578±23 (34%)	632±26 (37%)	683±44 (29%)

^{a} Due to the 0-0 transition of free chains. ^{b} Due to the 0-0 transition of aggregated chains. ^{c} Due to the 0-1 transition of aggregated chains. ^{d} Intensity percentage of each curve.
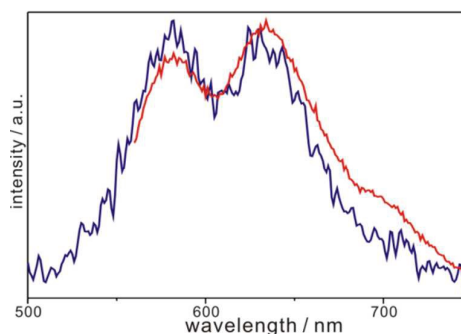
Fig. 4 Emission spectra of thick NFs (b) in cyclohexanone with excitation at 355 (blue) and 532 nm (red).

In aggregate P3HT systems such as films and NFs, the excited state is split into two different energy states due to the existence of inter- (H-type) or intrachain (J-type) aggregation.[13,14] Since the excitation energy is another critical factor associated with the formation of the split excited states of NFs,[14,37] we have also obtained the emission spectra of NFs with excitation at 532 nm (Fig. S6 of ESI†). As shown in Table 1 and Fig. S6 of ESI†, each emission spectrum of both thin and thick NFs in cyclohexanone with excitation at 532 nm has been deconvoluted into three Gaussian curves having the maxima at 577, 632, and 686 nm. With decreasing excitation energy from 3.49 eV (355 nm) to 2.33 eV (532 nm), the intensity fraction of the 0-0 transition of free or amorphous chains has been found to decrease. The $I_{em}^{0-0}/I_{em}^{0-1}$ of thin NFs (2.3) is 1.8 times greater than that of thick NFs (1.3). In comparison, difference between the $I_{em}^{0-0}/I_{em}^{0-1}$ values of thin and thick NFs in emission spectra with excited at 532 nm is smaller than that with excitation at 355 nm. In Fig. 4, we definitely show that the emission spectra of NFs are quite sensitive to excitation

energy. Compared with the 0-0 transition of free or amorphous chains at ~580 nm, the 0-0 transition of aggregated chains at ~630 nm is weaker with excitation at 355 nm but stronger with excitation at 532 nm. Furthermore, the 0-1 vibronic transition of aggregated chains at ~690 nm is eminent with excitation at 532 nm.
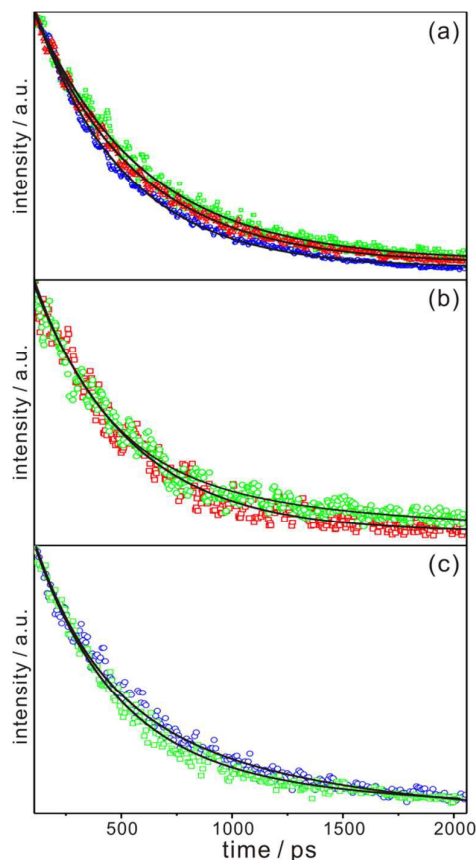
Fig. 5 Emission kinetic profiles of thick NFs excited at 355 nm and monitored at 580 (blue), 650 (green), and 690 nm (red) (a), thin (green) and thick NFs (red) excited at 355 nm and monitored at 650 nm (b), and thick NFs excited at 355 (blue) and 532 nm (green) and monitored at 650 nm (c). NFs were dispersed in cyclohexanone, and solid lines are best-fitted curves to extract kinetic constants.

Fig. 5a shows the emission kinetic profiles of thick NFs are quite dependent on the monitored wavelengths. We have assigned the decay times monitored at 580 nm of 433 ps for thick NFs and 440 ps for thin NFs to the decay of the relaxed S_1 excitons of non-aggregated P3HT chains (Table 2).[25,26,30] Intrachain or interchain energy transfer (~20 and ~100 ps)[26] has been hardly observed because its time scale is similar to our instrument response time (25 ps). Meanwhile, emission at 650 and 690 nm arises from the recombination of the relaxed S_1 excitons of aggregated P3HT chains. High intrachain or interchain aggregation within NFs can form a higher singlet exciton state (quasi-continuous band) via the singlet exciton-exciton annihilation (singlet fusion, Scheme 2)[14] due to the increase of interactions between adjacent S_1 excitons in highly ordered regions. Thus, as shown in Table 2, the emission kinetic profile of thick NFs monitored at 650 nm has been

deconvoluted into two decay components of 280 ps (55%) and 1100 ps (45%) while that monitored at 690 nm has two decay components of 250 ps (45%) and 900 ps (55%). Since the shorter decay is much faster than the recombination of normal relaxed S_1 excitons, this process has been assigned to the biexciton recombination; the recombination of one S_1 exciton increases the recombination probability of adjacent S_1 excitons.[39] The longer decay component of ~1500 ps is due to the increased delocalization of relaxed S_1 excitons induced by intrachain aggregation associated with the regioregularity and planarity of polymer chains.[11,39] Overall, the emission decay kinetic constants of NFs at 690 nm are found to be shorter than those at 650 nm because two-dimensional interchain effect inducing the nongeminate recombination of relaxed S_1 excitons is more important at 690 nm than at 650 nm (Table 2).

Table 2. Emission Decay Kinetic Constants of NFs Dispersed in Cyclohexanone

sample	λ_{ex} (nm)	λ_{mon} (nm)	I_0[a]	decay time (ps)	mean time (ps)
thin NFs	355	580	1.00	440	440
		650	0.16	320 (70%) + 1800 (30%)	584
		690	0.30	300 (57%) + 920 (43%)	567
	532	580	0.97	420	420
		650	0.07	380 (81%) + 2000 (19%)	633
		690	0.09	370 (80%) + 1100 (20%)	516
thick NFs	355	580	0.56	433	433
		650	0.13	280 (55%) + 1100 (45%)	649
		690	0.26	250 (45%) + 900 (55%)	607
	532	580	1.00	420	420
		650	0.04	340 (78%) + 1800 (22%)	661
		690	0.08	330 (75%) + 1100 (25%)	522
pristine NFs	355	580	1.00	400	400
		650	0.20	340 (75%) + 1000 (25%)	505
		690	0.27	330 (70%) + 900 (30%)	501

[a] Relative initial intensity.

As shown in Fig. 5b and Table 2, the emission kinetic profile of thin NFs excited at 355 nm and monitored at 650 nm decays slower than that of thick NFs. High intrachain aggregation in J-type P3HT NFs has been reported to form delocalized S_1 excitons, inducing nongeminate recombination. On the other hand, lower intrachain aggregation in H-type P3HT NFs forms localized S_1 excitons, inducing faster geminate recombination dominantly.[11] However, since our thick NFs have both coupling types of H-aggregate and J-aggregate, the

recombination of relaxed S_1 excitons, faster than that in thin NFs, can be attributed to the probability increase of the nongeminate recombination of relaxed S_1 excitons due to interchain aggregation along the longitudinal axis. Since the probability of interactions between adjacent S_1 excitons increases in thick NFs, the interchain mixing occurs more efficiently in thick NFs than in thin NFs. Therefore, the fraction of the fast decay component in thin NFs is greater than that in thick NFs. This result indicates that other charge-carriers such as polaron pairs and polarons are generated rapidly from higher singlet exciton states produced by the interchain mixing (singlet fusion) in competition with the vibrational relaxation of S_1 excitons (Scheme 2).[14]

As discussed in Fig. 4, since the excitation energy affects the excited state of NFs, we have also obtained the emission kinetic profiles of our NFs with excitation at 532 nm (Fig. 5c). With decreasing excitation energy from 3.49 eV (355 nm) to 2.33 eV (532 nm), the fraction of the fast decay component increases in the emission kinetic profiles of both thin and thick NFs (Table 2). This result also suggests that the formation of a higher singlet exciton state associated with the fast decay component can be controlled by two critical factors: the excitation energy and the coupling type of NFs. As shown in Table 2, the emission decay kinetic profiles of pristine NFs excited at 355 nm and monitored at 650 and 690 nm have been also obtained. Compared to thin NFs, the decay time of the slow component monitored at 650 nm is shorter and the fraction of the fast component monitored at 690 nm is smaller. These results also indicate that non-aggregated or amorphous chains are predominant in pristine NFs. Although we have concentrated our attention on the decay dynamics of relaxed S_1 excitons, from now on, we will focus on the formation pathway and the decay dynamics of polaron pairs (PP), localized (LP), delocalized polarons (DP), and triplet (T_1) excitons in NFs.

Femtosecond transient-absorption (TA) spectra of aggregate P3HT systems such as films and NFs have been diversely reported[13-15,40b,41-44] to understand the formation and decay of charge carriers such as excitons, PP, LP, and DP. Photoinduced absorption bands around 660, 740, 820, 1000, and 1200 nm have been assigned to PP, DP, T_1 excitons, LP, and S_1 excitons, respectively.[14,40b,41] Thus, as shown in Fig. 6 and Fig. S7 of ESI†, we have obtained picosecond TA kinetic profiles of NFs at various probe wavelengths from 660 nm to 1200 nm to gain a profound insight into the excited-state absorption species of NFs. Fig. S7 of ESI† observed in time windows of 50 ps shows that although initial TA signals at 0 ps have been observed definitely, any rise components have not been observed. This suggests that in competition with vibrational relaxation to S_1 excitons (~1 ps) the fast formation of PP, DP, and LP takes place from higher singlet exciton states. Each TA kinetic profile of PP absorption at 660 nm in Fig. 6a observed in time windows of 1000 ps has been deconvoluted into two decay components of 18 ps (74%) and 212 ps (26%) for thin NFs and 34 ps (78%) and 463 (22%) for thick NFs (Table 3). We have assigned the fast decay component (0.7 ps for thin NFs and 0.6 ps for thick NFs) to the downhill relaxation of self-

trapped excitons (Table S2 of ESI†) and the medium decay component (14 and 18 ps for thin NFs and 16 and 34 ps for thick NFs) to torsional relaxation or intra/interchain energy transfer (Table 3 and Table S2 of ESI†).[28-30] Especially, as shown in Fig. 6a, the decay curve of PP of thin NFs is quite different from that of thick NFs. Since PP is an electron-hole pair bound by Coulomb interaction, this species often recombines geminately. As discussed with emission decay constants, interchain aggregation effect induces the delocalization of S_1 excitons in association with nongeminate recombination. The decay time constant of PP in thin NFs (212 ps) has been found to be smaller than that in thick NFs (463 ps) because interchain aggregation is weaker than intrachain aggregation.
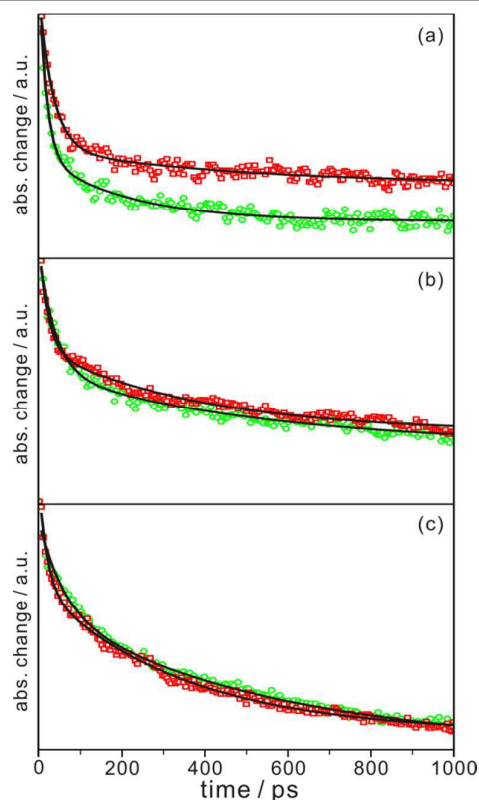
Fig. 6 Picosecond transient-absorption kinetic profiles of thin NFs (green) and thick NFs (red) excited at 355 nm and probed at 660 (a), 740 (b), and 1000 nm (c). NFs were dispersed in cyclohexanone, and solid lines are best-fitted curves to extract kinetic constants.

Table 3. Transient-Absorption Kinetic Constants of NFs Dispersed in Cyclohexanone with Excitation at 355 nm

sample	window (ns)	λ_{pr} (nm)	$A_0{}^a$ (10^{-3})	decay time (ps)
thin NFs	1	660	1.74	18 (74%) + 212 (26%)
		740	1.86	39 (63%) + 523 (37%)
		820	3.70	27 (48%) + 359 (52%)
		1000	7.40	58 (37%) + 535 (63%)
		1200	1.80	20 (40%) + 310 (60%)
	1000	820	48.6	307,000
thick NFs	1	660	1.66	34 (78%) + 463 (22%)
		740	2.00	21 (51%) + 383 (49%)
		820	3.45	22 (66%) + 616 (34%)
		1000	7.70	20 (33%) + 345 (67%)
		1200	2.82	20 (35%) + 290 (65%)
	1000	820	51.5	322,000
pristine NFs	1	660	1.20	17 (53%) + 291 (47%)
		740	1.68	36 (58%) + 526 (42%)
		820	3.12	49 (44%) + 2418 (56%)
		1000	8.10	32 (34%) + 395 (66%)
		1200	2.13	18 (33%) + 358 (67%)
	1000	820	61.6	283,000

^{a} Initial transient absorbance

The TA decay curves of DP and LP, namely free charge carriers, have been obtained for thin and thick NFs (Fig. 6b,c). It has been reported[41] that DP bands originate from mobile polarons in ordered P3HT regions (lamellar structures with enhanced interchain coupling), whereas LP bands arise from localized polarons in disordered P3HT regions. Similarly, in our NFs, because the two-dimensional interchain effect induces the formation of DP, the initial transient absorbance of thick NFs in a time window of 50 ps is larger than that of thin NFs (Table S2 of ESI†). The hot-exciton dissociation model is another important factor affecting the formation of LP and DP.[14] In other words, the formation of LP and DP is dependent on excitation energy. Since we have used one kind of excitation wavelength (355 nm), this phenomenon has not been observed in our TA kinetic profiles of NFs. However, in emission kinetic profiles of Fig. 5c, as we have varied excitation wavelengths, this phenomenon has been observed (see the discussion of Fig. 5c). Each TA kinetic profile of DP absorption at 740 nm in Fig. 6b has been deconvoluted into two decay components of 39 ps (63%) and 523 ps (37%) for thin NFs and 21 ps (51%) and 383 ps (49%) for thick NFs. Unlike the decay dynamics of PP, the decay time constant of DP in thin NFs has been found to be smaller than that in thick NFs. The decay dynamics of LP is similar to that of DP; each TA kinetic profile

of LP absorption at 1000 nm in Fig. 6c has been deconvoluted into two decay components of 58 ps (37%) and 535 ps (63%) for thin NFs and 20 ps (33%) and 345 ps (67%) for thick NFs. Because P is a free-charge carrier, it recombines non-geminately. As thick NFs have both coupling types of H-aggregate and J-aggregate, the probability of the nongeminate recombination of free-charge carriers such as DP and LP increases due to the effect of interchain aggregation along the longitudinal axis, resulting in the faster recombination of DP and LP than in thin NFs. Meanwhile, Table 3 and Table S2 of ESI† also show the fast (downhill relaxation of self-trapped excitons) and the medium (torsional relaxation or intra/interchain energy transfer) decay components of DP and LP in both thin and thick NFs. As polaron is a free-charge carrier, the decay times of DP and LP in thick NFs are found to be shorter than the respective ones in thin NFs. On the other hand, because PP is an electron-hole pair bound by Coulomb interaction, the decay of PP in thick NFs is found to be slower than that in thin NFs.[44] As shown in Table 3 and Fig. S7 of ESI†, we have also obtained the TA kinetic profiles of NFs at 1200 nm; each TA kinetic profile of S_1 absorption at 1200 nm has been deconvoluted into two decay components of 20 ps (40%) and 310 ps (60%) for thin NFs and 20 ps (35%) and 290 ps (65%) for thick NFs. We have assigned the fast decay component of 20 ps to intra/interchain energy transfer.[26] Since the slow decay times are nearly consistent with the emission decay time constant of relaxed S_1 excitons, the slow component has been considered to originate from the decay of relaxed S_1 excitons, which is faster in thick NFs than in thin NFs due to interchain delocalization effect enhancing nongeminate recombination. As shown in Table 3, we have also obtained picosecond TA kinetic profiles of pristine NFs to understand the role of Au NPs in the charge-carrier dynamics of NFs. If the formation of S_1 excitons in NFs is inhibited by Au NPs via energy or charge transfer, the initial transient absorbance of S_1 excitons of thin NFs containing Au NPs would be significantly smaller than that of pristine NFs. However, the initial transient absorbance of S_1 excitons at 1200 nm of thin NFs is slightly smaller than that of pristine NFs, whereas the initial transient absorbances of PP and DP at 660 and 740 nm, respectively, of thin NFs are even larger than the respective ones of pristine NFs. These results suggest that Au NPs hardly hinder the formation of S_1 excitons in NFs.
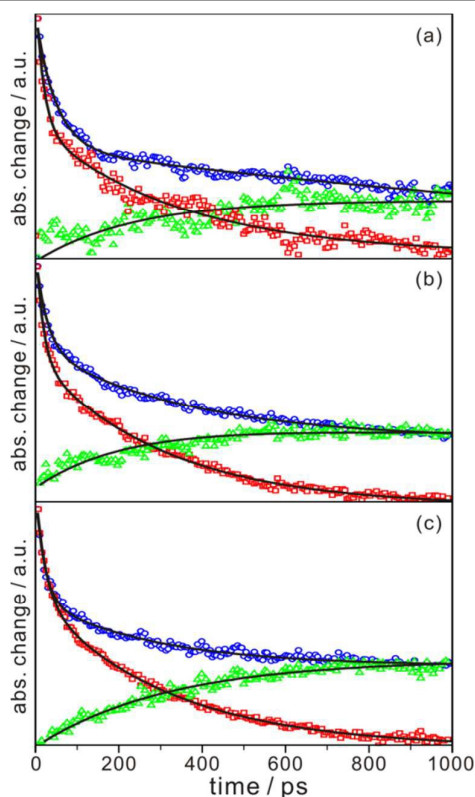
Fig. 7 Picosecond transient-absorption kinetic profiles of pristine NFs (a), thin NFs (b), and thick NFs (c) excited at 355 nm and monitored at 820 (blue) and 1200 nm (red). Green triangles in each panel have been obtained by subtracting red squares from blue circles. Solid lines are best-fitted curves to extract time constants.

Unlike S_1 excitons, T_1 excitons have the advantage of a long lifetime ($10^{-6} \sim 10^{-3}$ s), expanding the diffusion length associated with optoelectronic-device performances. Because T_1 excitons are usually generated in a small amount in conjugated polymers, formation mechanisms, such as singlet fission,[14] intersystem crossing (ISC),[25,28] and nongeminate recombination of delocalized polaron species,[11] of T_1 excitons have been studied to overcome the low density of T_1 excitons. We have obtained TA kinetic profiles at 820 nm to gain the information of T_1 excitons; each TA kinetic profile in Fig. 7 and Fig. S7 of ESI† has been deconvoluted into two decay components (Table 3 and Table S2 of ESI†). As shown in Fig. 7, we have obtained the rise curves (green triangles) associated with formation dynamics of T_1 excitons by subtracting the TA decay profiles of S_1 absorption at 1200 nm from the TA decay profiles of S_1 and T_1 absorption at 820 nm.[14] The formation time constants of 200 ps for pristine NFs, 250 ps for thin NFs, and 380 ps for thick NFs have been obtained via fitting exponential functions of $-A_r \exp(-t/\tau_r) + A_d \exp(-t/\tau_d) + B$ to the rise curves of Fig. 7. The obtained rise times are considerably shorter than a reported ISC time (1.2 ns).[28] As interchain mixing related to the formation of PP and DP occurs less efficiently in pristine NFs than in both thin and thick NFs, T_1 formation via singlet fission from a higher singlet exciton state occurs faster and more efficiently in pristine NFs than in both thin and thick NFs (Scheme 2). The threshold energy

requirement for the singlet fission has been reported as two thermalized T_1 excitons ($2ET_1$).[14] The energy level of the lowest T_1 exciton state (ET_1) has been estimated to be 1.43 eV for pristine NFs and 1.40 eV for both thin and thick NFs from the energy level of the lowest S_1 exciton state (ES_1) and the energy gap between ES_1 and ET_1 (ΔE_{ST}),[14] as the energy level of the lowest S_1 exciton state has been calculated from absorption spectra as 1.88 eV for pristine NFs and 1.84 eV for both thin and thick NFs and the singlet-triplet splitting energy ΔE_{ST} has been reported to be 0.45 eV for highly ordered poly(3-octylthiophene) films. Therefore, the threshold energy for the singlet fission has been estimated as 2.86 eV for pristine NFs and 2.80 eV for both thin and thick NFs. Because we used 355 nm (3.49 eV) as the excitation wavelength, the singlet fission could be observed in our TA kinetic profiles of NFs. In the next discussion, we will clearly suggest that T_1 excitons in NFs are mainly produced through the singlet fission rather than through ISC.
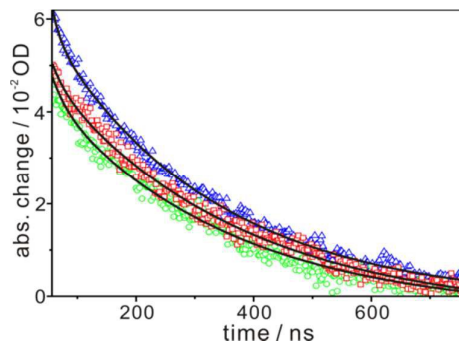
Fig. 8 Nanosecond transient-absorption kinetic profiles of pristine NFs (blue), thin NFs (green), and thick NFs (red). Samples were excited at 355 nm and probed at 820 nm. Solid lines are best-fitted curves to extract time constants.

We have also obtained nanosecond time-resolved TA kinetic profiles of NFs to support the formation path way of T_1 excitons in NFs (Fig. 8). Each TA kinetic profile of T_1 absorption at 820 nm has been deconvoluted into a single decay component (Table 3). The T_1 absorption kinetic profiles of non-aggregated P3HT and Au@P3HT NPs in chloroform have been reported30 to have a lifetime of ~235 ns, which is considerably smaller than the T_1 decay times of our NFs. In both thin and thick NFs, because the threshold energy for the singlet fission is 2.80 eV, T_1 excitons were hardly observed with excitation at 532 nm (2.33 eV) on a nanosecond time scale. In addition, the initial TA signals at 820 nm of thin and thick NFs are not larger than that of pristine NFs, suggesting that most T_1 excitons in NFs are not generated through ISC. Therefore, we conclude that T_1 excitons in our prepared NFs are mainly generated through the singlet fission from a higher singlet exciton state produced by the singlet fusion.

4 Conclusions

The formation and decay dynamics of S_1 and T_1, PP, and LP and DP dependent on the aggregate types of NFs has been

comprehensively investigated by time-resolved emission and TA spectroscopy. The thickness of NFs associated with a transition in dominant exciton coupling from intrachain to interchain coupling has been facilely tuned via controlling the concentration of Au@P3HT NPs in cyclohexanone. The emission ratio of the 0-0 transition to the 0-1 vibronic transition of thin NFs (4.2) having thickness of 15 nm is 2.5 times greater than that of thick NFs (1.7) having thickness of 25 nm, indicating that the J-aggregate character is predominant in thin NFs, whereas the H-aggregate character becomes as important as the J-aggregate character in thick NFs. With increasing excitation energy, the fraction of the fast emission decay component has been found to decrease, suggesting that the fast formation of localized PP, LP, and DP results from higher singlet exciton states produced by the singlet fusion. Since thick NFs have both coupling types of H-aggregates and J-aggregates, the faster recombination of relaxed S_1 excitons in thick NFs than in thin NFs can be attributed to the increased nongeminate recombination of relaxed S_1 excitons due to interchain aggregation. The faster decay dynamics of DP and LP in thick NFs than in thin NFs is due to the larger interchain stacking effect inducing the delocalization of DP and LP. As interchain aggregation is weaker than intrachain aggregation, PP decays faster in thin NFs than in thick NFs. The initial TA signal of S_1 excitons of thin NFs is slightly smaller than that of pristine NFs whereas the initial TA signals of PP and DP of thin NFs are even larger than the respective ones of pristine NFs, suggesting that Au NPs hardly hinder formation of S_1 excitons. The formation time of T_1 excitons was considerably shorter than a reported ISC time, and T_1 excitons were hardly observed with excitation at 532 nm on a nanosecond time scale. However, T_1 excitons have been observed with excitation at 355 nm. The initial TA signal of pristine NFs on a nanosecond time scale is larger than those of thin and thick NFs. Thus, T_1 excitons within our prepared NFs are mainly generated through the singlet fission from a higher singlet exciton state rather than through ISC from the lowest S_1 exciton state.

Acknowledgements

Notes and references

1   (a) C. Noguez, *J. Phys. Chem. C,* 2007, **111**, 3806–3819. (b) P. C. Ray, *Chem. Rev.*, 2010, **110**, 5332–5365.
2   J.-Y. Kim, D. Lee, H. J. Kim, I. Lim, W. I. Lee and D.-J. Jang, *J. Mater. Chem. A*, 2013, **1**, 5982–5988.
3   H.-B. Kim and D.-J. Jang, *CrystEngComm*, 2012, **14**, 6946–6951.
4   S. J. Kim, C. S. Ah and D. J. Jang, *Adv. Mater.*, 2007, **19**, 1064–1068.
5   W. U. Huynh, J. J. Dittmer and A. P. Alivisatos, *Science*, 2002, **295**, 2425–2427.
6   D. H. Park, M. S. Kim and J. Joo, *Chem. Soc. Rev.*, 2010, **39**, 2439–2452.
7   P. Reiss, E. Couderc, J. De Girolamo and A. Pron, *Nanoscale*, 2011, **3**, 446–489.
8   E. Stratakis and E. Kymakis, *Mater. Today*, 2013, **16**, 133–146.
9   H. Sirringhaus, P. Brown, R. Friend, M. M. Nielsen, K. Bechgaard, B. Langeveld-Voss, A. Spiering, R. A. Janssen, E. Meijer and P. Herwig, *Nature*, 1999, **401**, 685-688.
10 S.-J. Park, S.-G. Kang, M. Fryd, J. G. Saven and S.-J. Park, *J. Am. Chem. Soc.*, 2010, **132**, 9931-9933.
11 A. K. Thomas, J. A. Garcia, J. Ulibarri-Sanchez, J. Gao and J. K. Grey, *ACS Nano*, 2014, **8**, 10559-10568.
12 M. D. Barnes and M. Baghar, *J. Polym. Sci. Pol. Phys.*, 2012, **50**, 1121-1129.
13 J. Guo, H. Ohkita, H. Benten and S. Ito, *J. Am. Chem. Soc.*, 2010, **132**, 6154–6164.
14 J. Guo, H. Ohkita, H. Benten and S. Ito, *J. Am. Chem. Soc.*, 2009, **131**, 16869–16880.
15 H. Ohkita, S. Cook, Y. Astuti, W. Duffy, S. Tierney, W. Zhang, M. Heeney, I. McCulloch, J. Nelson and D. D. Bradley, et al. *J. Am. Chem. Soc.*, 2008, **130**, 3030–3042.
16 G. Nagarjuna, M. Baghgar, J. A. Labastide, D. D. Algaier, M. D. Barnes and D. Venkataraman, *ACS Nano*, 2012, **6**, 10750-10758.
17 S. Huettner, M. Sommer, J. Hodgkiss, P. Kohn, T. Thurn-Albrecht, R. H. Friend, U. Steiner and M. Thelakkat, *ACS Nano*, 2011, **5**, 3506-3515.
18 M. He, L. Zhao, J. Wang, W. Han, Y. Yang, F. Qiu and Z. Lin, *ACS Nano*, 2010, **4**, 3241-3247.
19 J. B. Gilroy, D. J. Lunn, S. K. Patra, G. R. Whittell, M. A. Winnik and I. Manners, *Macromolecules*, 2012, **45**, 5806-5815.
20 S. Berson, R. De Bettignies, S. Bailly and S. Guillerez, *Adv. Func. Mater.*, 2007, **17**, 1377-1384.
21 D. A. Kamkar, M. Wang, F. Wudl and T.-Q. Nguyen, *ACS Nano*, 2012, **6**, 1149-1157.
22 J. Xu, J. Hu, X. Liu, X. Qiu and Z. Wei, *Macromol. Rapid Commun.*, 2009, **30**, 1419-1423.
23 F. S. Kim and S. A. Jenekhe, *Macromolecules*, 2012, **45**, 7514-7519.
24 (a) S. Y. Choi, J. U. Lee, J. W. Lee, S. Lee, Y. J. Song, W. H. Jo and S. H. Kim, *Macromolecules*, 2011, **44**, 1771-1774. (b) J. S. Kim, J. H. Lee, J. H. Park, C. Shim, M. Sim and K. Cho, *Adv. Funct. Mater.*, 2011, **21**, 480-486. (c) T. Shimomura, T. Takahashi, Y. Ichimura, S. Nakagawa, K. Noguchi, S. Heike and T. Hashizume, *Phys. Rev. B*, 2011, **83**, 115314.
25 S. Cook, A. Furube and R. Katoh, *Energ. Environ. Sci.*, 2008, **1**, 294–299.
26 B. Ferreira, P. F. da Silva, J. S. r. Seixas de Melo, J. o. Pina and A. n. Maçanita, *J. Phys. Chem. B*, 2012, **116**, 2347–2355.
27 (a) G. Grancini, D. Polli, D. Fazzi, J. Cabanillas-Gonzalez, G. Cerullo and G. Lanzani, *J. Phys. Chem. Lett.*, 2011, **2**, 1099–1105. (b) G. Grancini, M. Biasiucci, R. Mastria, F. Scotognella, F. Tassone, D. Polli, G. Gigli and G. Lanzani, *J. Phys. Chem. Lett.*, 2012, **3**, 517–523.
28 (a) N. Banerji, S. Cowan, E. Vauthey and A. J. Heeger, *J. Phys. Chem. C*, 2011, **115**, 9726–9739. (b) N. Banerji, J. Seifter, M. Wang, E. Vauthey, F. Wudl and A. J. Heeger, *Phys. Rev. B*, 2011, **84**, 075206.
29 Y. Xie, Y. Li, L. Xiao, Q. Qiao, R. Dhakal, Z. Zhang, Q. Gong, D. Galipeau and X. Yan, *J. Phys. Chem. C*, 2010, **114**, 14590–14600.
30 D. Lee and D.-J. Jang, *Polymer*, 2014, **55**, 5469-5476.
31 T. Xu, M. Yan, J. D. Hoefelmeyer and Q. Qiao, *RSC Adv.*, 2012, **2**, 854-862.

ARTICLE

32 (a) J. A. Labastide, M. Baghgar, I. Dujovne, B. H. Venkatraman, D. C. Ramsdell, D. Venkataraman and M. D. Barnes, *J. Phys. Chem. Lett.*, 2011, **2**, 2089-2093. (b) T. J. Magnanelli and A. E. Bragg, *J. Phys. Chem. Lett.*, 2015, **6**, 438-445.

33 (a) F. C. Spano and C. Silva, *Annu. Rev. Phys. Chem.*, 2014, **65**, 477-500. (b) H. Yamagata and F. Spano, *J. Chem. Phys.*, 2012, **136**, 184901. (c) F. C. Spano, *Acc. Chem. Res.*, 2009, **43**, 429-439.

34 M. Baghgar, J. A. Labastide, F. Bokel, R. C. Hayward and M. D. Barnes, *J. Phys. Chem. C*, 2014, **118**, 2229-2235.

35 (a) E. T. Niles, J. D. Roehling, H. Yamagata, A. J. Wise, F. C. Spano, A. J. Moule and J. K. Grey, *J. Phys. Chem. Lett.*, 2012, **3**, 259-263. (b) F. Panzer, M. Sommer, H. Bässler, M. Thelakkat and A. Köhler, *Macromolecules*, 2015, **48**, 1543-1553.

36 M. Baghgar, A. M. Barnes, E. Pentzer, A. J. Wise, B. A. Hammer, T. Emrick, A. D. Dinsmore and M. D. Barnes, *ACS Nano*, 2014, **8**, 8344-8349.

37 M. Baghgar, J. Labastide, F. Bokel, I. Dujovne, A. McKenna, A. M. Barnes, E. Pentzer, T. Emrick, R. Hayward and M. D. Barnes, *J. Phys. Chem. Lett.*, 2012, **3**, 1674-1679.

38 C. Carach and M. Gordon, *J. Phys. Chem. B*, 2013, **117**, 1950–1957.

39 J. A. Labastide, M. Baghgar, A. McKenna and M. D. Barnes, *J. Phys. Chem. C*, 2012, **116**, 23803-23811.

40 (a) J. Gao, A. Kamps, S.-J. Park and J. K. Grey, *Langmuir*, 2012, **28**, 16401-16407. (b) T. P. Martin, A. J. Wise, E. Busby, J. Gao, J. D. Roehling, M. J. Ford, D. S. Larsen, A. J. Moulé and J. K. Grey, *J. Phys. Chem. B*, 2012, **117**, 4478-4487. (c) Z. Hu, T. Adachi, R. Haws, B. Shuang, R. J. Ono, C. W. Bielawski, C. F. Landes, P. J. Rossky and D. A. Vanden Bout, *J. Am. Chem. Soc.*, 2014, **136**, 16023-16031.

41 I.-W. Hwang, D. Moses and A. J. Heeger, *J. Phys. Chem. C*, 2008, **112**, 4350-4354.

42 A. R. S. Kandada, G. Grancini, A. Petrozza, S. Perissinotto, D. Fazzi, S. S. K. Raavi and G. Lanzani, *Sci. Rep.*, 2013, **3**, 2073.

43 Y. Tamai, Y. Matsuura, H. Ohkita, H. Benten and S. Ito, *J. Phys. Chem. Lett.*, 2014, **5**, 399-403.

44 Y. Ogata, D. Kawaguchi and K. Tanaka, *Sci. Rep.*, 2015, **5**, 8436.